

The phase diagram of ultra quantum liquids

Dam Thanh Son,¹ Mikhail Stephanov,² and Ho-Ung Yee^{2,1}

¹*Kadanoff Center for Theoretical Physics,
University of Chicago, Chicago, IL 60637, USA*

²*Department of Physics, University of Illinois, Chicago, IL 60607, USA*

We discuss the dependence of the phase diagram of a hypothetical isotope of helium with nuclear mass less than 4 atomic mass units. We argue that with decreasing nucleus mass, the temperature of the superfluid phase transition (about 2.2 K in real ^4He) increases, while that of the liquid-gas critical point (about 5.2 K in real ^4He) decreases. We discuss various scenarios that may occur when the two temperatures approach each other and the order parameters of the superfluid and the liquid-gas phase transitions interact with each other. The simplest scenario, in which both order parameters become critical at particular values of the nuclear mass, temperature, and pressure, can be ruled out through an analysis of the Landau theory. We argue that in the most likely scenario, as the nuclear mass decreases, first, a tricritical point appears on the line separating the superfluid and the normal fluid phase, then the critical point disappears under the first-order part of superfluid phase transition line, and in the end the tricritical point disappears. The last change in the phase diagram occurs when the two-body scattering length crosses zero, which corresponds to the nuclear mass of about 1.55 u. We develop a quantitative theory that allows one to determine the phase diagram in the vicinity of this point. Finally, we discuss several ways to physically realize such liquids.

I. INTRODUCTION

Helium is a prototypical quantum liquid, being the only natural substance that remains liquid down to zero temperature [1]. The reason for this behavior is the weakness of the interatomic potential and the smallness of the atomic mass, leading to large zero-point fluctuations destroying the would-be crystal.

The phase diagram of ^4He is schematically depicted in Fig. 1. The solid phase at high pressure has been left out of the phase diagram; we focus on the gas, the normal fluid, and the superfluid phases. There are two characteristic temperatures that can be seen from this phase diagram. The first is the temperature of the superfluid-to-normal phase transition, T_λ . This phase transition is second order and occurs at roughly $T \approx 2.2$ K (the temperature depends slightly on the pressure). The second temperature is the temperature of the liquid-gas critical point, T_c which is at approximately 5.2 K.

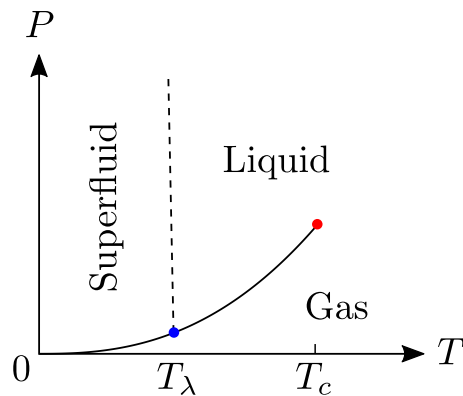


FIG. 1: The schematic phase diagram of physical ^4He . The solid phase at higher pressure is outside of the frame. Solid lines denote first-order phase transitions, dashed lines denote second-order phase transitions.

One can ask whether this phase diagram should be expected for any fluid which becomes a superfluid at low temperature. (Here by “fluid” we mean a thermodynamic system that has a liquid-gas phase transition terminated at a critical point. Typically, such a system is made out of particles which interact with each other through a potential with a van-der-Waals-type long-distance attractive tail and a short-range repulsive core.) Because helium is a unique liquid that becomes a superfluid at low temperature, this question is rarely asked. But one can, for example, inquire if the liquid-gas critical point can be made to lie inside the superfluid phase.

In this paper we try to establish the possible phase diagrams of an “ultra-quantum liquid,” which can be thought of as a hypothetical isotope of helium with a bosonic nucleus lighter than the ^4He nucleus (the alpha particle). Assuming that the mass of the nucleus is still much larger than the mass of the electron, one can use the Born-Oppenheimer approximation to treat the motion of the nuclei. In particular, the interaction potential between the atoms

remains unchanged. For the purpose of our discussion, which is focused on the qualitative features of the phase diagram, we can replace the exact interaction potential between the helium atoms by the Lennard-Jones potential

$$V(r) = 4\epsilon \left[\left(\frac{\sigma}{r} \right)^{12} - \left(\frac{\sigma}{r} \right)^6 \right], \quad (1)$$

which reaches a minimum of $-\epsilon$ at $r = 2^{1/6}\sigma$. We expect that the precise form of the potential should not matter much for qualitative questions; the potential (1) can be replaced by any potential with a r^{-6} long-distance tail and a short-distance repulsive core.

The magnitude of quantum effects is parametrized by the de Boer parameter [2]

$$\Lambda = \frac{\hbar}{\sigma\sqrt{m\epsilon}}. \quad (2)$$

In the WKB approximation, Λ is inversely proportional to the number of bound states that the potential supports, so a larger Λ corresponds to a more quantum system. The standard values of the Lennard-Jones parameters for helium are [3]

$$\sigma = 2.556 \text{ \AA}, \quad \epsilon/k_B = 10.22 \text{ K}. \quad (3)$$

For the physical mass $m = m_{\text{phys}} = 4 \text{ u}$, $\Lambda \approx 0.426$. (For comparison, hydrogen H_2 has the de Boer parameter of about 0.275 and is thus less quantum than ${}^4\text{He}$.)

Often one defines the van der Waals length through the coefficient of the r^{-6} tail of the potential, $V(r) \sim -C_6 r^{-6}$ as $r \rightarrow \infty$, as

$$\ell_{\text{vdW}} = \frac{1}{2} \left(\frac{mC_6}{\hbar^2} \right)^{1/4}. \quad (4)$$

A particle rolling down the $C_6 r^{-6}$ potential from infinity with zero energy acquires a WKB phase of order unity when it reaches the radius ℓ_{vdW} . The de Boer parameter can be written as

$$\Lambda = \frac{\sigma^2}{2\ell_{\text{vdW}}^2}. \quad (5)$$

As m decreases, Λ increases. Now, since the quantum effects are more enhanced than in ${}^4\text{He}$, we expect that the ground state at zero temperature and zero pressure is not a solid for all $m < m_{\text{phys}}$. We want to understand, at the qualitative level at least, what happens to the phase diagram as the fluid becomes more quantum. (Previously, the effect of changing the nuclear mass on the zero-temperature ground state of helium has been studied in Refs. [4–6].)

Qualitatively, one may speculate that the hierarchy $T_\lambda < T_c$ may no longer hold as m decreases. Very roughly, the superfluid phase transition can be interpreted as the Bose-Einstein condensation, which occurs at temperature

$$T_{\text{BEC}} = \frac{\hbar^2 n^{2/3}}{m}. \quad (6)$$

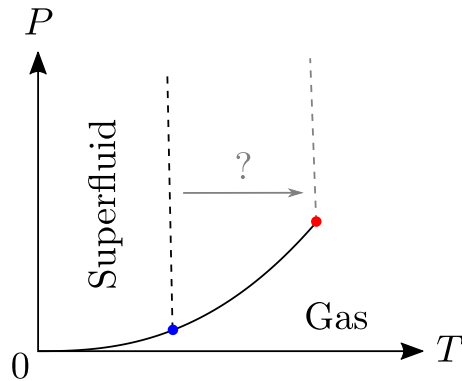


FIG. 2: The hypothetical simplest scenario. We show that it is not realized.

Assuming that the density n of the fluid does not change much (which is a reasonable assumption since the distance between atoms in the liquid phase is determined by the location of the minimum of the interatomic potential σ), with decreasing m then the superfluid transition occurs at higher and higher temperature.

On the other hand, for a classical gas the m dependence of the thermal partition function can be completely factored out, so the location of the critical point should be independent of the nuclear mass. But when the critical temperature is not much larger than the temperature of the superfluid phase transition, one needs to take into account quantum effects on the position of the critical point. Studies of the isotopic dependence of the critical point show that the critical temperature decreases with decreasing mass (or increasing de Boer parameter) [7]. So at some value of the mass m the superfluid transition temperature may become equal or even larger than than the liquid-gas critical temperature. How does the phase diagram look like then?

The simplest scenario is depicted in Fig. 2. As m decreases the distance between the critical end point (the point and the critical point becomes smaller, and vanishes at some value of m . At this critical value of m then, both the superfluid and the liquid-gas order parameters would become critical at the same point on the (P, T) phase diagram.

In this paper we rule out this simplest scenario. We argue that as the nuclear mass is lowered, the following succession of changes in the topology of the phase diagram occurs. The boundary between different regimes are denoted as m_1, m_2, m_3 .

- For $m_1 < m < m_{\text{phys}}$ the phase diagram is topologically the same as that of the physical ${}^4\text{He}$ (Fig. 1).
- For $m_2 < m < m_1$ a tricritical point appears on the line of the superfluid phase transition. The superfluid phase transition, instead of being always second-order, is now first-order at low pressure and second order at high pressure. The junction between the superfluid, normal fluid and gas phases is now a triple point instead of being a critical endpoint [8] (Fig. 3a).

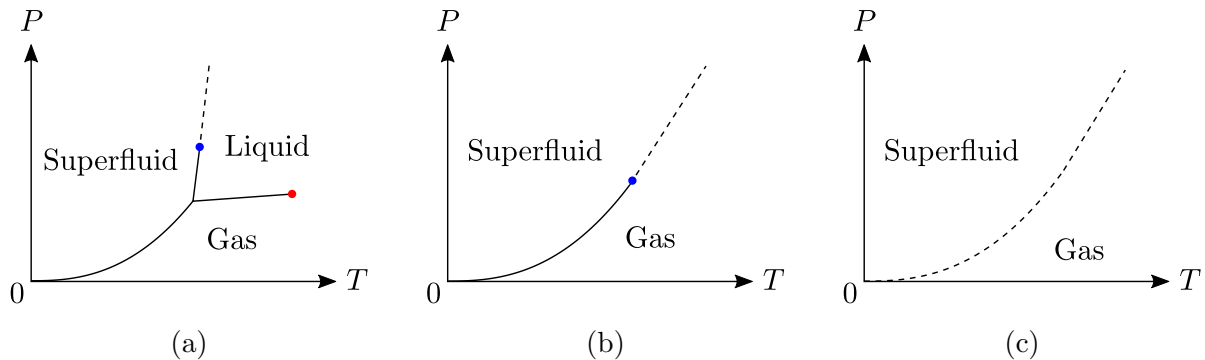


FIG. 3: The evolution of the phase diagram as one lowers the atomic mass.

- When $m_3 < m < m_2$, the liquid gas critical point disappears under the first-order superfluid phase transition line. The phase diagram now has two phases, a superfluid phase and a normal phase, separated by the line of phase transitions which are first-order at low pressure and second-order at high pressure (Fig. 3b).
- For $m < m_3$ the tricritical point disappears, and the whole line of superfluid phase transition is second order (Fig. 3c).

While m_1 and m_2 cannot be computed analytically, the value of m_3 can be determined: it is the value of the mass for which the scattering length for the two-atom scattering vanishes. For helium this happens when m is 1.55 atomic units. Thus, all the transformations of the phase diagram described above happen in a relatively narrow window of nuclear mass, ranging from 1.55 to 4 atomic units.

II. ANALYSIS OF THE MEAN-FIELD THEORY

A. Ruling out the simplest scenario

We now show that the simplest scenario, in which at a critical value of the mass the phase diagram looks like in Fig. 2, is excluded. In this scenario one would have a multicritical point with $O(2) \times Z_2$ symmetry. We first analyze this hypothetical multicritical point from the point of view of Landau's theory of phase transition.

We introduce two order parameters: the superfluid condensate ψ and the liquid-gas order parameter ϕ . The condensate ψ is complex and the free energy is supposed to have $U(1)$ symmetry $\psi \rightarrow \psi e^{i\alpha}$. On the other hand, there is no symmetry associated with the order parameter ϕ of the liquid-gas phase transition, which can be taken to be the density. Writing down all terms in the free energy to fourth order in the expansion in powers of ψ and ϕ , we get the most general expression

$$\Omega(\psi, \phi) = \frac{t}{2}\phi^2 + \frac{u}{4}\phi^4 - h\phi + (t + \tilde{m})|\psi|^2 + \frac{\lambda}{2}|\psi|^4 - \alpha\phi|\psi|^2 - \gamma\phi^2|\psi|^2. \quad (7)$$

Here we have eliminated the (redundant) ϕ^3 term by using the freedom to shift ϕ by an arbitrary constant $\phi \rightarrow \phi + c$ (note that there is no symmetry $\phi \rightarrow -\phi$).

The $O(2) \times Z_2$ multicritical point is achieved when the coefficients of $t = \tilde{m} = h = \alpha = 0$. This requires fine tuning of four variables, while we can change only three parameters (the temperature, the pressure, and the mass of the nucleus). Therefore, the $O(2) \times Z_2$ multicritical point cannot be achieved.

The argument given above is essentially based on mean-field theory neglecting critical fluctuations. To show that our conclusion remains valid beyond the mean-field level, one needs to show that each of the six fixed points [9] of the model has *more than three* $O(2)$ -symmetric (but not necessarily Z_2 symmetric) relevant operators. Let us do that first for the $O(3)$ fixed point, where an enhanced symmetry combines the superfluid order parameter ψ and liquid-gas order parameter (appropriately shifted and rescaled) χ into a $O(3)$ vector: $\Phi_a \sim (\text{Re } \psi, \text{Im } \psi, \phi)$. The $O(3)$ fixed point has the following relevant operators, ordered by the rank of the representation of the $SO(3)$ group [10],

$$\begin{aligned} \Phi^2 &\equiv \Phi_a \Phi_a; \\ \Phi_a &; \\ \Phi_{ab} &= \Phi_a \Phi_b - \frac{1}{3} \delta_{ab} \Phi^2; \\ \Phi_{abc} &= \Phi_a \Phi_b \Phi_c - \frac{1}{5} \Phi^2 (\delta_{bc} \Phi_a + \delta_{ca} \Phi_b + \delta_{ab} \Phi_c). \end{aligned} \tag{8}$$

All these operators have dimensions below 3; for example, the dimension of the operator Φ_{abc} has been estimated to be close to 2 [10]. (In addition, the rank-4 operator $\Phi_{abcd} = \Phi_a \Phi_b \Phi_c \Phi_d + \dots$ may be very weakly relevant [11]). Restricting only to $O(2)$ symmetric-operators, we have the following relevant operators at the $O(3)$ fixed point

$$\begin{aligned} \Phi^2 &\sim |\psi|^2 + \phi^2; \\ \Phi_3 &\sim \phi; \\ \Phi_{33} &\sim 2\phi^2 - |\psi|^2; \\ \Phi_{333} &\sim 2\phi^3 - 3|\psi|^2\phi. \end{aligned} \tag{9}$$

(There would be one more relevant operator if the rank-4 operator is relevant at the $O(3)$ -invariant fixed point.) Thus there are at least four relevant operators at the $O(3)$ symmetric fixed point.

The other coupled fixed point is the biconical fixed point [9]. This fixed point was found to be very close to the $O(3)$ critical point [11], so the operators (9) should be relevant also at the biconical fixed point. Thus one also needs *at least four* fine-tuned parameters to reach this fixed point. The analysis can be performed easily at the other four fixed points, where the order parameters decouple and the operator dimensions are just sums of operators dimensions in the Z_2 and $O(2)$ theories. One concludes that there is no $O(2) \times Z_2$ fixed point that can be approached by fine-tuning three $O(2)$ symmetric parameters.

B. The overall evolution of the phase diagram

To understand what actually happens as one lowers the nuclear mass, we analyze the mean-field theory based on the free energy (7). For simplicity we set $\gamma = 0$ and rescale the fields so that $\alpha = 1$. The thermodynamic potential in a grand canonical ensemble (the negative of pressure) that needs to be minimized in the phase diagram in (t, h) space is

$$\Omega(\phi, |\psi|) = \frac{t}{2}\phi^2 + \frac{u}{4}\phi^4 - h\phi + (t + \tilde{m})|\psi|^2 + \frac{\lambda}{2}|\psi|^4 - \phi|\psi|^2. \quad (10)$$

Here, (u, λ) are assumed to be positive constants, but \tilde{m} is a variable parameter that can have any sign, and is presumably related to the mass of a helium atom. The (t, h) should be related to the conventional parameters (T, μ) in the ordinary phase diagram.

We now investigate numerically the evolution of the phase diagram of the model given by Eq. (10) as a function of \tilde{m} . To find the minimum of the free energy, one first notices that Ω is quadratic in $|\psi|^2$, so it is easy to “integrate out” ψ , which results in the replacement in Eq. (10) of $|\psi|^2$ by its value at the minimum given by

$$|\psi|^2 = \frac{1}{\lambda}(\phi - \tilde{m} - t)\theta(\phi - \tilde{m} - t), \quad (11)$$

where $\theta(x)$ is the Heaviside step function. Then the resulting effective potential for ϕ becomes

$$V(\phi) = \frac{t}{2}\phi^2 + \frac{u}{4}\phi^4 - h\phi - \frac{1}{2\lambda}(\phi - \tilde{m} - t)^2\theta(\phi - \tilde{m} - t). \quad (12)$$

By minimizing $V(\phi)$ we find the Z_2 order parameter $\langle\phi\rangle$, and then use (11) to obtain the superfluid order parameter $\langle|\psi|^2\rangle$.

The 3D plots on Fig. 4 show the values of each order parameter in the (t, h) space, $\langle\phi\rangle(t, h)$ and $\langle|\psi|^2\rangle(t, h)$. In the plots one can see discontinuous jumps represent first-order phase transition lines. The second-order phase transition lines for superfluid order can also be seen. We can play with changing the parameter \tilde{m} to see how the phase transition lines change.

The numerical result can be summarized as follows. For sufficiently large \tilde{m} , that is $\tilde{m} > \tilde{m}_1$, the phase diagram is similar to that of the physical ${}^4\text{He}$. As \tilde{m} drops below \tilde{m}_1 , a modification appears on the line of the superfluid phase transition: the lower part of the line (which touches the liquid-gas phase transition line) becomes first order, the upper part remains second order. The two parts are separated by a tricritical point. As \tilde{m} drops further, when $\tilde{m} < \tilde{m}_2$ liquid-gas critical point disappears under the first-order superfluid-to-normal phase transition line (Fig. 3b).

C. The appearance of the superfluid tricritical point

One can understand qualitatively why the superfluid phase transition becomes first-order when this transition happens close to the liquid-gas phase transition in the following manner.

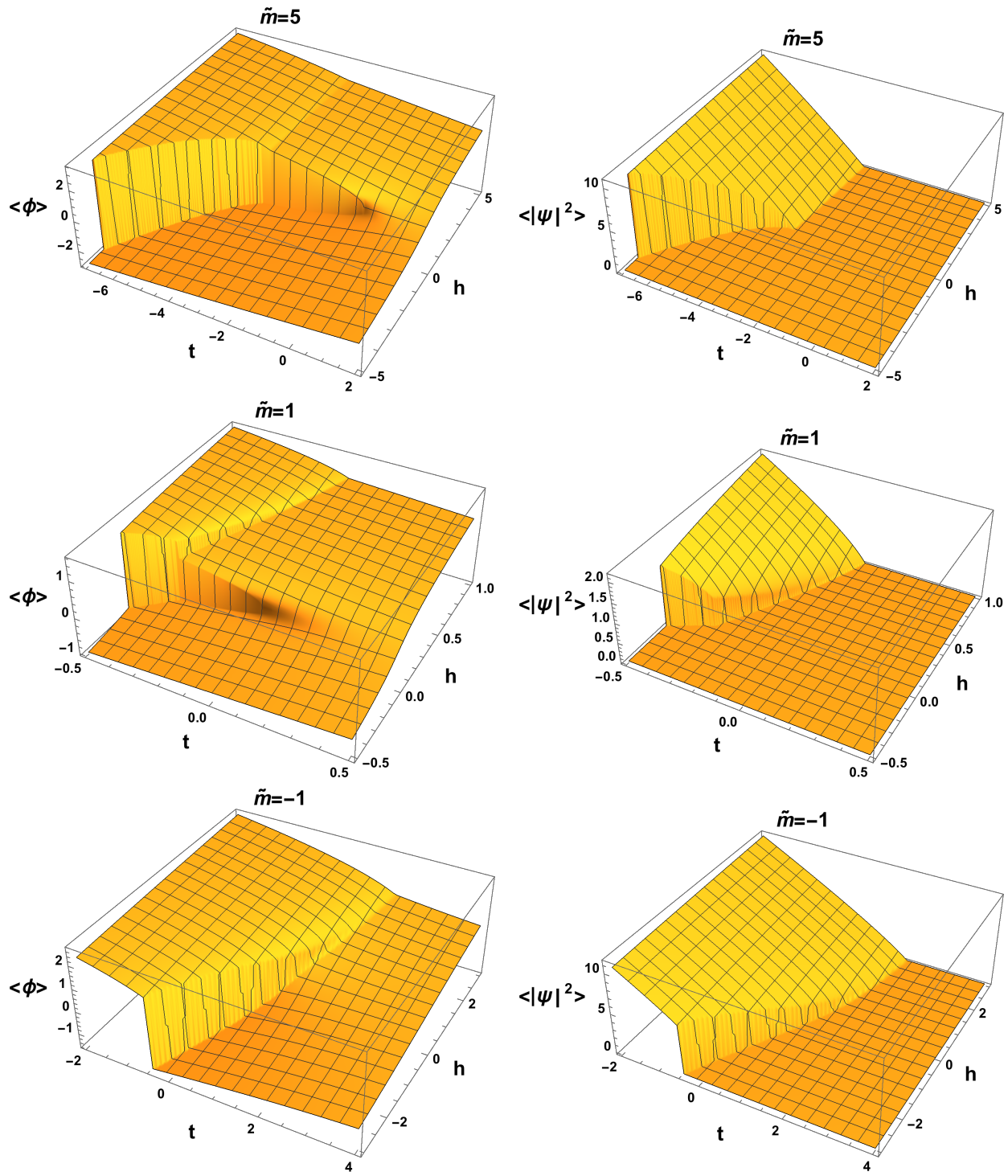


FIG. 4: The order parameters $\langle \phi \rangle$ (left) and $\langle |\psi|^2 \rangle$ (right) in (t, h) space, for $u = 1$, $\lambda = 1/2$ and $\tilde{m} = 5, 1$ and -1

Suppose we expand the potential around the minimum at ϕ_0 , i.e., $\phi = \phi_0 + \delta\phi$. Then the potential contains the following terms:

$$V(\phi, \psi) = \dots + \frac{1}{2\chi}(\delta\phi)^2 - \delta\phi|\psi|^2 + \frac{\lambda}{2}|\psi|^4, \quad (13)$$

where χ is the susceptibility of the system with respect to the order parameter ϕ . Let us “integrate out” the fluctuations of the liquid-gas order parameter ϕ to obtain an effective potential for ψ . One then finds

$$V_{\text{eff}}(\psi) = \dots + \left(\frac{\lambda}{2} - \frac{\chi}{2}\right) |\psi|^4. \quad (14)$$

As one approaches the critical point, the susceptibility $\chi \rightarrow \infty$ and $|\psi|^4$ coefficient turns negative. This means that the superfluid phase transition will have to become a first-order phase transition. In other words, the coupling between the superfluid order parameter and the liquid-gas order parameter drives the superfluid phase transition first-order when the latter occurs near the liquid-gas critical point.

One can use the argument above to locate the point $\tilde{m} = \tilde{m}_1$ where the superfluid tricritical point starts to appear. At this \tilde{m} the tricritical point is located on the line of the liquid gas phase transition, on the liquid side: $t < 0$, $h = +0$. The average value of the liquid-gas order parameter at this point is

$$\langle \phi \rangle = \phi_0 = \sqrt{-\frac{t}{u}}. \quad (15)$$

Expanding $\phi = \phi_0 + \delta\phi$, the potential becomes

$$V = (-t)\delta\phi^2 + u\phi_0\delta\phi^3 + (t + \tilde{m} - \langle \phi \rangle)|\psi|^2 + \frac{\lambda}{2}|\psi|^4 - \delta\phi|\psi|^2. \quad (16)$$

Integrating out $\delta\phi$ means that we minimize the potential with respect to $\delta\phi$ at fixed ψ . We have to solve

$$\frac{\partial V}{\partial \delta\phi} = 2(-t)\delta\phi + 3u\phi_0\delta\phi^2 - |\psi|^2 = 0. \quad (17)$$

This equation can be solved for small $|\psi|$:

$$\delta\phi = \frac{|\psi|^2}{2(-t)} - \frac{3u\phi_0}{8(-t)^3}|\psi|^4 + O(|\psi|^6). \quad (18)$$

Putting this back into the potential, we find the effective potential for ψ :

$$V_{\text{eff}}(\psi) = (\tilde{m} + t - \phi_0)|\psi|^2 + \left(\frac{\lambda}{2} - \frac{1}{4(-t)}\right) |\psi|^4 + \frac{u\phi_0}{8(-t)^3}|\psi|^6 + O(|\psi|^8). \quad (19)$$

At the tricritical point the coefficients of the $|\psi|^2$ and $|\psi|^4$ terms vanish, which means

$$t = -\frac{1}{2\lambda}, \quad \tilde{m}_1 = \frac{1}{\sqrt{2\lambda u}} + \frac{1}{2\lambda}. \quad (20)$$

Note that at this point the coefficient of the $|\psi|^6$ term is positive, so this *is* the tricritical point. For example, for $\lambda = \frac{1}{2}$ and $u = 1$, $\tilde{m}_1 = 2$, consistent with the numerical results in Fig. 4.

D. Disappearance of the liquid-gas critical point

Now let us find the value of \tilde{m}_2 at which the liquid-gas critical point is located on the line of the (first-order) superfluid phase transition. At the liquid-gas critical point, we have $t = h = 0$, since it is always located in the normal phase side where coupling to superfluid plays no role. The normal phase $\phi = \psi = 0$ must have the same free energy as the superfluid phase. As discussed above, the free energy in the superfluid phase is the minimum of the effective potential

$$V_{\text{eff}}(\phi) = \frac{u}{4}\phi^4 - \frac{1}{2\lambda}(\phi - \tilde{m})^2, \quad (21)$$

and the system of equations we need to solve is

$$V_{\text{eff}}(\phi) = \frac{u}{4}\phi^4 - \frac{1}{2\lambda}(\phi - \tilde{m}_2)^2 = 0, \quad V'_{\text{eff}}(\phi) = u\phi^3 - \frac{1}{\lambda}(\phi - \tilde{m}_2) = 0. \quad (22)$$

The solution is

$$\phi = \frac{1}{\sqrt{2u\lambda}}, \quad \tilde{m}_2 = \frac{1}{2\sqrt{2u\lambda}}. \quad (23)$$

For example, when $u = 1$, $\lambda = 1/2$, $\tilde{m}_2 = \frac{1}{2}$. Note that $\tilde{m}_1 > \tilde{m}_2$, so as one lowers the atomic mass the superfluid tricritical point appears before the liquid-gas critical point disappears.

Of course, the mean field model cannot be more than just a guide for us to guess the correct result, which needs to be obtained by a more rigorous method. However, as we will see in the next Section, the phase diagram depicted in Fig. 3b is realized in a regime where reliable calculations can be performed. As a direct transformation from Fig. 1 to Fig. 3b is impossible, the overall picture suggested by the mean-field analysis appears to be the simplest one possible.

III. FINAL DISAPPEARANCE OF THE SUPERFLUID TRICRITICAL POINT: THE UNBINDING PHASE TRANSITION

Further evolution of the phase diagram can be determined, approaching the problem from another end: from the regime of very small nuclear mass. Here one expects that very strong zero-point fluctuations make the liquid unbound: the density of the zero-temperature superfluid goes to zero in the limit of zero pressure. In this case the superfluid-normal phase boundary should be completely second order, as in a dilute Bose gas with repulsive interaction. Thus, the tricritical point in Fig. 3b moves to lower and lower temperature and pressure as one decreases the nuclear mass, and completely disappears at some value of the latter.

The transition between the phase diagram topologies sketched on Fig. 3b and Fig. 3c occurs when the scattering length characterizing the low-energy scattering between two atoms crosses zero [12, 13]. For the Lennard-Jones potential, as the de Boer parameter Λ increases, the scattering length $a(\Lambda)$ goes through a series of poles and zeros (see, e.g., Ref. [14]). The last pole of $a(\Lambda)$ occurs at $\Lambda \approx 0.423$; the physical mass of the ^4He isotope is

very close to this value. The largest zero of $a(\Lambda)$ is $\Lambda \approx 0.679$, and this corresponds to the nuclear mass of about 1.58 u. Using the more realistic Aziz potentials [15, 16], we obtain a slightly lower numerical value of 1.55 u for the nuclear mass at which a vanishes.

As m approaches m_3 from above, the tricritical point moves to zero temperature and zero pressure. The density of the superfluid and the normal gas phases on the two sides of the first-order section of the superfluid phase transition is small, therefore one can use effective field theory to describe this phase transition.

A. Dilute liquid at zero temperature

At zero temperature, the problem of the dilute droplets of bosons with small two-body coupling and finite three-body coupling has been considered in Refs. [13, 17]. (Dilute quantum droplets have recently been considered in the context of trapped bosons [18–22], but unlike our system, these droplets are stabilized by effects beyond mean field.) For completeness, we rederive the relevant formulas here.

At zero temperature the free energy density, as a function of particle number density n , is given by

$$\frac{\Omega}{V} = \frac{g}{2}n^2 + \frac{G}{6}n^3 - \mu n, \quad (24)$$

where

$$g = \frac{4\pi\hbar^2 a}{m}, \quad G = \frac{\hbar^2 D}{m}, \quad (25)$$

a is the scattering length and D is the three-body scattering hypervolume [23, 24]. The scattering length a approaches zero when the de Boer parameter Λ approaches the critical value $\Lambda_c \approx 0.679$ as [25]

$$a \approx 3.82812 \ell_{\text{vdW}}(\Lambda - \Lambda_c) \approx 2.23 \left(\frac{\Lambda}{\Lambda_c} - 1 \right) \sigma. \quad (26)$$

We will work in the regime $a < 0$, $|a| \ll \sigma$. The three-body scattering hypervolume D has been computed for the Lennard-Jones potential at $\Lambda = \Lambda_c$ [25]

$$D = (86 \pm 2) \ell_{\text{vdW}}^4 \approx 47\sigma^4. \quad (27)$$

For $g < 0$ a first-order phase transition occurs at the value of μ where local minimum of the free energy (24) is equal to the free energy of the vacuum, i.e., zero:

$$-|g|n + \frac{G}{2}n^2 - \mu = 0, \quad (28)$$

$$-\frac{|g|}{2}n^2 + \frac{G}{6}n^3 - \mu n = 0. \quad (29)$$

These equations have the solution

$$n_0 = \frac{3(-g)}{2G} = 6\pi \frac{(-a)}{D}, \quad (30)$$

$$\mu_0 = -\frac{3g^2}{8G} = -\frac{6\pi^2\hbar^2 a^2}{mD}. \quad (31)$$

These formulas coincide with those obtained Refs. [13, 17].

B. Field-theory calculation at finite temperature

We now investigate the phase diagram of the Bose gas for small and negative g , concentrating on the first-order superfluid phase transition. We start with the Euclidean Lagrangian for a non-relativistic boson with chemical potential μ

$$\mathcal{L}_E = \psi^\dagger \partial_\tau \psi - \frac{\hbar^2}{2m} |\nabla \psi|^2 - \mu \psi^\dagger \psi + \frac{g}{2} (\psi^\dagger \psi)^2 + \frac{g'}{2} |\nabla(\psi^\dagger \psi)|^2 + \frac{G}{6} (\psi^\dagger \psi)^3. \quad (32)$$

Here in addition to the two- and three-point interactions with coupling constants g and G , we have introduced an interaction involving extra two spatial derivatives with strength g' . By matching the scattering amplitude obtained from the Lagrangian with the effective range expansion, one finds that g' is proportional to the effective range r_0 of the potential,

$$g' = \frac{\pi \hbar^2}{m} a^2 r_0. \quad (33)$$

Note that when $a \rightarrow 0$, generically r_0 diverges as a^{-2} so that g' remains finite [26]. From dimensional analysis we expect $a^2 r_0 \sim \sigma^3$. Numerically, we find for the Lennard-Jones potential at $\Lambda = \Lambda_c$,

$$\lim_{\Lambda \rightarrow \Lambda_c} a^2 r_0 \approx 5.13 \ell_{\text{vdW}}^3 \approx 3.23 \sigma^3. \quad (34)$$

Normally, at small density the interaction term proportional to g dominates, but since the coefficient of this term, g , is tuned to zero, one needs to take into account interactions which involve more particles (G) or more derivatives (g'). As we shall discuss in more detail below, in the regime of our interest, the addition of a pair of operators ψ^\dagger and ψ brings a suppression factor of $|a|/\sigma$, and a pair of spatial derivatives a factor of $(|a|/\sigma)^{2/3}$.

We expand the field in Fourier modes of Matsubara frequency and momentum,

$$\psi(\tau, \mathbf{x}) = \sum_{n \in \mathbb{Z}} e^{-\frac{2\pi i n \tau}{\beta}} \psi_n(\mathbf{x}) = \sum_{n \in \mathbb{Z}} e^{-\frac{2\pi i n \tau}{\beta}} \int_{\mathbf{k}} e^{i\mathbf{k} \cdot \mathbf{x}} \psi_{n, \mathbf{k}}, \quad (35)$$

where $\beta \equiv 1/T$ and

$$\int_{\mathbf{k}} \equiv \int \frac{d^3 \mathbf{k}}{(2\pi)^3}. \quad (36)$$

The Euclidean action then has the form

$$\begin{aligned} S_E/\beta &= \int_{\mathbf{k}} \sum_n \psi_{n, \mathbf{k}}^* \left(-\frac{2\pi i n}{\beta} + \frac{\hbar^2 \mathbf{k}^2}{2m} - \mu \right) \psi_{n, \mathbf{k}} \\ &+ \frac{g}{2} \int_{\mathbf{x}} \sum_{n_1, n_2, n_3, n_4} \psi_{n_1}^* \psi_{n_2}^* \psi_{n_3} \psi_{n_4} \delta_{n_1+n_2-n_3-n_4} e^{\frac{2\pi i \varepsilon}{\beta} (n_1+n_2)} \\ &+ \frac{g'}{2} \int_{\mathbf{x}} \sum_{n_1, n_2, n_3, n_4} \nabla_i (\psi_{n_1}^* \psi_{n_3}) \nabla_i (\psi_{n_2}^* \psi_{n_4}) \delta_{n_1+n_2-n_3-n_4} e^{\frac{2\pi i \varepsilon}{\beta} (n_1+n_2)} \\ &+ \frac{G}{6} \int_{\mathbf{x}} \sum_{n_1, n_2, n_3, n_4, n_5, n_6} \psi_{n_1}^* \psi_{n_2}^* \psi_{n_3}^* \psi_{n_4} \psi_{n_5} \psi_{n_6} \delta_{n_1+n_2+n_3-n_4-n_5-n_6} e^{\frac{2\pi i \varepsilon}{\beta} (n_1+n_2+n_3)}, \quad (37) \end{aligned}$$

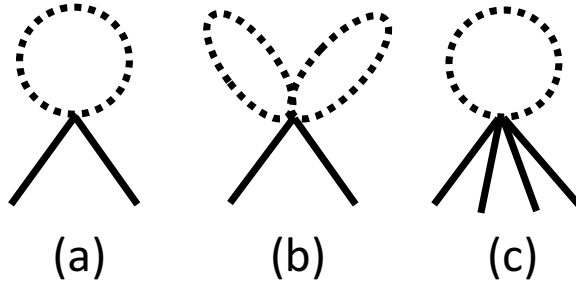


FIG. 5: The “tadpole” diagrams contributing to effective parameters in the 3D effective theory. Diagrams (a) and (b) contribute to μ_{eff} , diagram (a) with g' vertex to m_{eff} , and diagram (c) to g_{eff} (see Eq. (53)). Dashed lines are $n \neq 0$ modes that are integrated out.

where the last factor with $\varepsilon = 0^+$ is from the time ordering of $\psi^\dagger(\tau+\varepsilon)\psi(\tau)$ in the interaction terms that ensures the normal ordering of $\psi^\dagger\psi$ in the operator form.

One can now derive the Feynman rules for the theory. The free propagator is given by

$$\langle \psi_{n',\mathbf{k}'}^* \psi_{n,\mathbf{k}} \rangle = \frac{1}{-2\pi i n + \beta \left(\frac{\hbar^2 \mathbf{k}^2}{2m} - \mu \right)} (2\pi)^3 \delta(\mathbf{k}' - \mathbf{k}) \delta_{n'-n}. \quad (38)$$

The interaction terms in the Lagrangian in Eq. (32) generate three types of vertices: a four-point vertex $-2g\beta$, a four-point vertex equal to $g'\beta$ multiplied by

$$2(\mathbf{p}_1 \cdot \mathbf{p}_2 + \mathbf{k}_1 \cdot \mathbf{k}_2) - (\mathbf{p}_1 + \mathbf{p}_2) \cdot (\mathbf{k}_1 + \mathbf{k}_2) = -(\mathbf{p}_1 - \mathbf{k}_1)^2 - (\mathbf{p}_1 - \mathbf{k}_2)^2, \quad (39)$$

where the incoming momenta are denoted as $\mathbf{p}_1, \mathbf{p}_2$ and outgoing momenta as $\mathbf{k}_1, \mathbf{k}_2$, and a six-point vertex $-6G\beta$.

We integrate out $n \neq 0$ modes to obtain a three-dimensional effective field theory for the zero Matsubara frequency ($n = 0$) modes. As shown below and in the Appendices, the small parameter controlling the loop expansion is the ratio of the scattering length a to the range of the Lennard-Jones potential σ :

$$\frac{|a|}{\sigma} \ll 1. \quad (40)$$

There are two other relevant length parameters: the typical interparticle spacing $n^{-1/3}$ and the thermal length λ_T , given by

$$\lambda_T = \sqrt{\frac{2\pi\hbar^2}{mT}}. \quad (41)$$

However, in the regime we want to consider, i.e., densities of order n_0 and temperatures of order the tricritical temperature, both n_0 and λ_T are given in terms of a and the small parameter in Eq. (40). In particular, the density in the regime where we are working is

of order n_0 given in Eq. (30), and since, on dimensional grounds, the hypervolume D is of order σ^4 (see Eq. (27)), we see that $|a| \ll \sigma$ corresponds to the dilute limit:

$$n|a|^3 \sim \frac{a^4}{D} \sim \left(\frac{a}{\sigma}\right)^4 \ll 1. \quad (42)$$

The thermal length λ_T at the temperatures we are interested in, i.e., near the Bose-Einstein condensation transition, is of order the particle separation $n^{-1/3}$, and is thus also set in terms of the ratio in Eq. (40).

We find that in the regime $|a| \ll \sigma$ the tadpole diagrams dominate over other loop diagrams, as far as the determination of the tricritical point at T_{tri} and the first-order phase transition line for $T < T_{\text{tri}}$ is concerned. (We use the term ‘‘tadpole’’ for a diagram with an internal line which starts and ends at the same point, as in Fig. 5). Physically, the tadpoles correspond to thermal occupation of bosonic excitations above the condensate (the $n = 0$ mode). Integrating out tadpoles with $n \neq 0$ modes corresponds to incorporating the effects of the normal component on the dynamics of the superfluid condensate.

In Appendices A and B we show that non-tadpole diagrams with nonzero Matsubara frequency modes and the loop diagrams within the 3D effective field theory can be neglected in the regime we are considering, i.e., near the tricritical point for a system with $|a| \ll \sigma$.

There are two tadpole diagrams contributing to the corrections to the 3D effective parameter μ_{eff} , each coming from four-point and six-point interaction vertices. The contribution from the tadpoles with a four-point vertex is

$$\Delta\mu = - \int_{\mathbf{k}} (2g + g'\mathbf{k}^2) \sum_{n \neq 0} \frac{e^{\frac{2\pi i n \varepsilon}{\beta}}}{-2\pi i n + \beta \left(\frac{\hbar^2 \mathbf{k}^2}{2m} - \mu\right)}. \quad (43)$$

The numerator in Eq. (43) comes from the normal ordering of operators in the interaction vertices. If n summation included $n = 0$, the result would be simply the Bose-Einstein distribution function,

$$\sum_{n \in \mathbb{Z}} \frac{e^{\frac{2\pi i n \varepsilon}{\beta}}}{-2\pi i n + \beta \left(\frac{\hbar^2 \mathbf{k}^2}{2m} - \mu\right)} = \frac{1}{\exp \left[\beta \left(\frac{\hbar^2 \mathbf{k}^2}{2m} - \mu\right)\right] - 1}, \quad (44)$$

so the sum in Eq. (43) is simply this with $n = 0$ term subtracted,

$$\Delta\mu = - \int_{\mathbf{k}} (2g + g'\mathbf{k}^2) \left(\frac{1}{\exp \left[\beta \left(\frac{\hbar^2 \mathbf{k}^2}{2m} - \mu\right)\right] - 1} - \frac{1}{\beta \left(\frac{\hbar^2 \mathbf{k}^2}{2m} - \mu\right)} \right). \quad (45)$$

The first integral over \mathbf{k} is finite, but the second term is UV divergent. This divergence should cancel with the UV divergences in the loop diagrams of the 3D effective theory if the same regularization scheme is used in both calculations. It is convenient to use dimensional regularization, in which tadpoles do not have UV divergences. We have

$$\Delta\mu = - \frac{2g}{\lambda_T^3} L(\beta\mu) - \frac{6\pi g'}{\lambda_T^5} M(\beta\mu), \quad (46)$$

where

$$L(x) = \text{Li}_{3/2}(e^x) + \sqrt{-4\pi x}, \quad (47)$$

$$M(x) = \text{Li}_{5/2}(e^x) - \frac{4}{3}\sqrt{-\pi x^3}, \quad (48)$$

and the thermal wavelength λ_T is defined in Eq. (41).

The tadpole contribution to μ_{eff} from the six-point vertex is similarly computed to be

$$\Delta\mu = -\frac{3G}{\lambda_T^6}L^2(\beta\mu), \quad (49)$$

and the tadpole contribution to g_{eff} from the G -vertex is

$$\Delta g = \frac{3G}{\lambda_T^3}L(\beta\mu). \quad (50)$$

There is also a correction to the mass m :

$$\Delta\left(\frac{1}{m}\right) = \frac{2g'}{\hbar^2\lambda_T^3}L(\beta\mu) \quad (51)$$

Thus, the 3D effective theory is described by the Lagrangian

$$\mathcal{L}_{3\text{D}}/\beta = \frac{\hbar^2}{2m_{\text{eff}}}\left|\nabla\psi_0\right|^2 - \mu_{\text{eff}}\psi_0^\dagger\psi_0 + \frac{g_{\text{eff}}}{2}(\psi_0^\dagger\psi_0)^2 + \frac{G}{6}(\psi_0^\dagger\psi_0)^3, \quad (52)$$

with the parameters

$$\mu_{\text{eff}} = \mu - \frac{2g}{\lambda_T^3}L(\beta\mu) - \frac{6\pi g'}{\lambda_T^5}M(\beta\mu) - \frac{3G}{\lambda_T^6}L^2(\beta\mu), \quad (53a)$$

$$g_{\text{eff}} = g + \frac{3G}{\lambda_T^3}L(\beta\mu), \quad (53b)$$

$$\frac{1}{m_{\text{eff}}} = \frac{1}{m} + \frac{2g'}{\hbar^2\lambda_T^3}L(\beta\mu). \quad (53c)$$

As we show in Appendix B, the contributions of higher-derivative and higher-order terms are suppressed in the effective theory given by Eq. (52). The tadpole contributions in Eq. (53a) are described by diagrams in Fig. 5(a) with g and g' vertex, as well as the diagram in Fig. 5(b) with G vertex correspondingly. The tadpole contribution in Eq. (53b) is from the diagram in Fig. 5(b), and the tadpole contribution in Eq. (53c) is from the diagram in Fig. 5(a) with g' vertex.

The first order phase transition line is determined by solving the equation for $\mu(T)$,

$$\mu_{\text{eff}} = -\frac{3g_{\text{eff}}^2}{8G}, \quad (54)$$

and the tricritical point is at $g_{\text{eff}} = \mu_{\text{eff}} = 0$.

We will see that the most interesting regime is $|\beta\mu| \ll 1$ ($\beta\mu < 0$). In this regime, the functions $L(x)$ and $M(x)$ tend to constant values

$$L(\beta\mu) = \zeta\left(\frac{3}{2}\right) + \zeta\left(\frac{1}{2}\right)\beta\mu + \dots, \quad (55a)$$

$$M(\beta\mu) = \zeta\left(\frac{5}{2}\right) + \zeta\left(\frac{3}{2}\right)\beta\mu + \dots. \quad (55b)$$

Let us define

$$n_B(T) \equiv \zeta\left(\frac{3}{2}\right) \frac{1}{\lambda_T^3} = \zeta\left(\frac{3}{2}\right) \left(\frac{mT}{2\pi\hbar}\right)^{3/2}, \quad (56)$$

which is the density of a free Bose gas with temperature T and zero chemical potential. Now Eqs. (53) become

$$\mu_{\text{eff}} = \mu - 2gn_B(T) - 3Gn_B^2(T) - \frac{6\pi\zeta(\frac{5}{2})}{\zeta(\frac{3}{2})} \frac{1}{\lambda_T^2} g' n_B(T), \quad (57)$$

$$g_{\text{eff}} = g + 3Gn_B(T). \quad (58)$$

C. The tricritical point

The phase transition is first order when $T < T_{\text{tri}}$ and second order when $T > T_{\text{tri}}$, where the tricritical temperature T_{tri} is determined by requiring $g_{\text{eff}} = 0$:

$$T_{\text{tri}} = \frac{2\pi\hbar^2}{m} \left[\frac{(-g)}{3\zeta(\frac{3}{2})G} \right]^{2/3} = \frac{2\pi\hbar^2}{m} \left[\frac{4\pi(-a)}{3\zeta(\frac{3}{2})D} \right]^{2/3}. \quad (59)$$

The chemical potential at the tricritical point is determined from $\mu_{\text{eff}} = 0$. From Eqs. (57) and (59) it follows that

$$\mu_{\text{tri}} = 6\pi\zeta\left(\frac{5}{2}\right) g' \left(\frac{-g}{3\zeta(\frac{3}{2})G} \right)^{5/3} - \frac{1}{3} \frac{g^2}{G}. \quad (60)$$

In the limit $g \rightarrow 0$, the first term on the right-hand side of Eq. (60) dominates over the second term, and one can estimate

$$\mu_{\text{tri}} \sim \frac{\hbar^2 |a|^{5/3}}{m\sigma^{11/3}}. \quad (61)$$

One can now check that the condition $\beta\mu \ll 1$ is satisfied at the tricritical point:

$$\beta\mu \sim \frac{|a|}{\sigma} \ll 1. \quad (62)$$

The correction to the mass is also small:

$$\Delta\left(\frac{1}{m}\right) \sim \frac{g'}{\hbar^2 \lambda_T(T_{\text{tri}})} \sim \frac{1}{m} \frac{|a|}{\sigma} \ll \frac{1}{m} \quad (63)$$

One expects that (62) and (63) are valid not only at the tricritical point, but also in the whole regime of temperature and chemical potential $T \sim T_{\text{tri}}$, $\mu \sim \mu_{\text{tri}}$.

Since $|\mu| \ll T$, the particle number at the tricritical point is given by

$$n_{\text{tri}} = n_{\text{B}}(T_{\text{tri}}) = \frac{1}{3} \frac{(-g)}{G}. \quad (64)$$

This is equal to $\frac{2}{9}$ of the density of the liquid phase at zero temperature n_0 [Eq. (30)].

D. The first-order phase transition

For $T < T_{\text{tri}}$, the phase transition is first-order. Assuming that $T \sim T_{\text{tri}}$, then $\mu \sim \mu_{\text{tri}}$ and the condition $\beta\mu \ll 1$ is still valid. The chemical potential at the first-order phase transition is determined via

$$\mu_{\text{eff}} = -\frac{3}{8} \frac{g_{\text{eff}}^2}{G}. \quad (65)$$

Let us now compute the density along the coexistence curve. In the gas phase the density is equal to the density of a Bose gas with temperature T and zero chemical potential

$$n_{\text{gas}} = n_{\text{B}}(T) = \left(\frac{T}{T_{\text{tri}}}\right)^{3/2} n_{\text{tri}} = \frac{2}{9} \left(\frac{T}{T_{\text{tri}}}\right)^{3/2} n_0. \quad (66)$$

The density in the (superfluid) liquid phase is the sum of the condensate density and the density of the thermal excitations:

$$n_{\text{liq}} = n_{\text{cond}} + n_{\text{B}}(T), \quad (67)$$

where the condensate density is

$$n_{\text{cond}} = \frac{3}{2} \frac{(-g_{\text{eff}})}{G} = \frac{3}{2} \frac{(-g)}{G} - \frac{9}{2} n_{\text{B}}(T) = \frac{9}{2} \left[1 - \left(\frac{T}{T_{\text{tri}}}\right)^{3/2}\right] n_{\text{tri}}. \quad (68)$$

Therefore

$$n_{\text{liq}} = \left[\frac{9}{2} - \frac{7}{2} \left(\frac{T}{T_{\text{tri}}}\right)^{3/2}\right] n_{\text{tri}} = \left[1 - \frac{7}{9} \left(\frac{T}{T_{\text{tri}}}\right)^{3/2}\right] n_0. \quad (69)$$

Equations (66) and (67) describe the boundaries of the coexistence region on the T vs n phase diagram as shown in Fig. 6.

By minimizing the free energy given by Eq. (52) for a configuration interpolating between the two phases, one finds the profile of the superfluid order parameter on the interface,

$$\psi_0(x) = \sqrt{\frac{n_{\text{cond}}}{1 + e^{2x/\xi}}}, \quad \xi = \frac{1}{2\pi\sqrt{3}} \frac{D^{1/2}}{|a|} \left[1 - \left(\frac{T}{T_{\text{tri}}}\right)^{3/2}\right]^{-1}, \quad (70)$$

and the surface tension,

$$\tau = 3\sqrt{3}\pi^2 \frac{\hbar^2 a^2}{mD^{3/2}} \left[1 - \left(\frac{T}{T_{\text{tri}}}\right)^{3/2}\right]^2. \quad (71)$$

The surface tension vanishes as $(T_{\text{tri}} - T)^2$ and the thickness of the interface diverges as $(T_{\text{tri}} - T)^{-1}$ near T_{tri} .

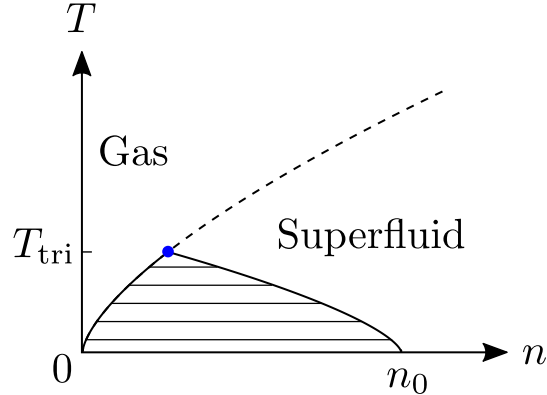


FIG. 6: The phase diagram in the temperature vs density plane corresponding to Fig. 3b.

	⁴ He	²⁰ Ne	⁴⁰ Ar	⁸⁴ Kr	H ₂	N ₂	O ₂	CO	CH ₄
M_{eq}	4	80.6	832	2790	9.50	545	722	595	517
$M_{\text{eq}}(\mu)$	0.020	0.412	4.23	14.1	0.051	2.79	3.69	3.04	2.68

TABLE I: Equivalent helium mass for selected substances and their muonic versions.

IV. POSSIBLE REALIZATIONS OF ULTRA QUANTUM LIQUIDS

In the real world the mass of the helium nucleus is fixed. There are two bosonic isotopes of helium, ⁶He and ⁸He, with half-lives of 0.8 s and 0.12 s, respectively. The lifetime of these isotopes is very large compared to the microscopic time scales and thus the question about the phase diagram of these isotopes make sense. The nuclear masses of these isotopes, however, lie on the other side of the mass of the ⁴He nucleus, compared to the mass region explored in this paper. The behavior of ⁶He and ⁸He must be more classical than that of ⁴He.

Substances other than helium have smaller de Boer parameter and hence are more classical. Let us define, for a given substance, the “equivalent helium mass” to be the mass of a helium isotope (measured in atomic mass unit) that would have the same de Boer parameter as that of the chosen substance:

$$M_{\text{eq}} = \frac{m}{m_N} \frac{\epsilon}{\epsilon_{\text{He}}} \left(\frac{\sigma}{\sigma_{\text{He}}} \right)^2. \quad (72)$$

The equivalent helium mass for selected substances are given on the second row of Table I, where we have used the Lennard-Jones parameters from Ref. [3].

One possible (but admittedly experimentally very difficult) way to achieve a de Boer parameter larger than that of ⁴He is to create “muonic matter” by replacing all electrons in a given substance by muons [27, 28]. The effect of this replacement is to increase the depth of the potential ϵ by a factor of the ratio of the muon mass m_μ to the electron mass m_e , $m_\mu/m_e \approx 207$, and to decrease the range of the potential σ by the same factor. This

has an effect of reducing the equivalent helium mass

$$M_{\text{eq}}(\mu) = \left(1 + \frac{Z}{A} \frac{m_\mu}{m_N}\right) \frac{m_e}{m_\mu} M_{\text{eq}}(e) \quad (73)$$

(we have taken into account a small change of the mass of the atom). The equivalent helium mass of the muonic substances are given in the third row of Table I. One can see that among the noble gases, muonic argon has essentially the same de Boer parameter as that of (electronic) ^4He , and thus will have a phase diagram very similar to that of ^4He (with the superfluid transition temperature of order 5000 K). At the same time muonic neon would be deep in the “gas-like” phase and muonic krypton and xenon should be rather classical. On the other hand, muonic N_2 , O_2 , CO and CH_4 have the equivalent helium mass within the interesting range (from 1.55 to 4) and hence can realize the various versions of the phase diagram treated in this paper.

Another type of exotic matter is formed when one replaces the protons in H_2 by a lighter positively charged particles, for example, muons or pions. Denoting the mass of the particle that replaces the proton as m , the equivalent helium mass of this substance would be

$$M_{\text{eq}} = 2m \frac{\sigma_{\text{H}_2}^2 \epsilon_{\text{H}_2}}{\sigma_{\text{He}}^2 \epsilon_{\text{He}}} \approx 9.50m \approx \frac{1}{193} \left(\frac{m}{m_e}\right) \text{u}. \quad (74)$$

According to this formula, when $m \approx 770m_e$ the substance would behave like helium, and when $m < 300m_e$, its phase diagram is that of a repulsive Bose gas.

Previously, Wheeler has put the estimate of the critical mass of the proton replacement at which the self-bound liquid disappears at $253 m_e$ [28]. One can try to determine this value better by using a more accurate interaction potential between two hydrogen molecules, for example, the widely used Silvera-Goldman potential [29] or the Buck potential [30]. It turns out that these potentials give results practically indistinguishable from Wheeler’s estimate ($250 m_e$ for the Silvera-Goldman potential and $256 m_e$ for the Buck potential). One can obtain a very good estimate almost analytically by noticing that the 10-6 potential

$$V(r) = c_{10-6} \epsilon \left[\left(\frac{\sigma}{r}\right)^{10} - \left(\frac{\sigma}{r}\right)^6 \right] \quad (75)$$

(where $c_{10-6} = 2^{-1}3^{-3/2}5^{5/2} \approx 5.379$ is chosen so that ϵ is the potential depth at its minimum) provides a considerably better approximation to the Silvera-Goldman and Buck potentials, compared to the 12-6 potential. The added advantage of the 10-6 potential is that the scattering length is known analytically in terms of potential parameters [31]; in particular, the last zero of a occurs at the value of the de Boer parameter $\Lambda = \hbar/\sigma\sqrt{2m\epsilon} = \sqrt{c_{10-6}}/3 \approx 0.773$. Using the core radius and the potential depth of the Silvera-Goldman potential, $\sigma = 2.974 \text{ \AA}$ and $\epsilon/k_B = 34.31 \text{ K}$, one obtains $m \approx 243 m_e$, surprisingly close to the result obtained by numerically integrating the Schrödinger equation, given the crudeness of the approximation.

From the estimate above, it appears that “muonium matter,” matter made out of muonium molecules $(\mu^+e^-)_2$ or Mu_2 , with $m_\mu/m_e \approx 207$, would not form a self-bound liquid

and would have a phase diagram of the type of a repulsive Bose gas, while the molecules $(\pi^+e^-)_2$, made out of positive pions and electrons with $m_{\pi^+}/m_e \approx 273$, is capable of forming a self-bound liquid. However, given the short lifetimes of the muon and the pion, perhaps a more realistic way to realize a quantum liquid of H_2 -like molecules is to use excitons in a solid where the hole and the electron have very different effective masses. When the ratio of the masses of the hole and the electron that form the exciton varies between approximately 250 and 800, the fluid of biexcitons [32] could realize different versions of the phase diagram discussed in this paper. This estimate will change if the mass tensors are anisotropic.

V. CONCLUSION

In this paper we have followed the evolution of the phase diagram of helium-4 as one dials the nucleus mass from the physical value of 4 u to a value where the scattering length vanishes, estimated to be 1.55 u. We have argued that the phase diagram goes through a sequence of changes before it finally becomes a quantum “gas-like” phase diagram, where there is only a single second-order phase transition between the superfluid and the normal phases.

Except for the last change in the phase diagram—the disappearance of the superfluid tricritical point—the values of the nuclear masses at which the intermediate changes of the phase diagram occur (the first appearance of the tricritical point and the disappearance of the liquid-gas critical point) cannot be obtained through simple calculations. Fortunately, this problem is free from the sign problem and can be studied using quantum Monte-Carlo simulations [33].

Much of the discussion of this paper should be relevant in a more general setting of van der Waals liquids, i.e., liquids consisting of particles which interact with each other through a potential which has a r^{-6} power-law decay at long distances and a repulsive core at short distances. It is possible that many features of the phase diagrams would remain the same for other exponents of the power-law tail of the potential. It would be also interesting to examine the possible phase diagrams of van der Waals quantum liquids in two dimensions.

The authors thank Massimo Boninsegni, Luca Delacrétaz, Youssef Kora, Sergej Moroz, Ana Maria Rey, Shiwei Zhang, and Wilhelm Zwerger for discussions and comments. This work is supported by the U.S. Department of Energy, Office of Science, Office of Nuclear Physics, within the framework of the Beam Energy Scan Theory (BEST) Topical Collaboration and grant No. DE-FG0201ER41195, by the U.S. DOE grant No. DE-FG02-13ER41958, by a Simons Investigator grant and by the Simons Collaboration on Ultra-Quantum Matter from the Simons Foundation.

[1] I.M. Khalatnikov, *An Introduction to the Theory of Superfluidity* (Benjamin, New York, 1965).

- [2] J. de Boer, “Quantum theory of condensed permanent gases. I. The law of corresponding states,” *Physica* **14**, 139–148 (1948).
- [3] Stephen Berry, Stuart A. Rice, and John Ross, *Physical Chemistry*, 2nd ed. (Oxford University Press, Oxford, UK, 2000).
- [4] L. H. Nosanow, L. J. Parish, and F. J. Pinski, “Zero-temperature properties of matter and the quantum theorem of corresponding states: The liquid-to-crystal phase transition for Fermi and Bose systems,” *Phys. Rev. B* **11**, 191–204 (1975).
- [5] M. D. Miller, L. H. Nosanow, and L. J. Parish, “Zero-temperature properties of matter and the quantum theorem of corresponding states. II. The liquid-to-gas phase transition for Fermi and Bose systems,” *Phys. Rev. B* **15**, 214–229 (1977).
- [6] J. Egger, E. Krotscheck, and R. E. Zillich, “Bose and Fermi Gases with Lennard-Jones Interactions,” *J. Low Temp. Phys.* **165**, 275–291 (2011).
- [7] Richard A. Young, “Theory of Quantum-Mechanical Effects at the Liquid-Gas Critical Point,” *Phys. Rev. Lett.* **45**, 638–641 (1980).
- [8] Michael E. Fisher and Marcia C. Barbosa, “Phase boundaries near critical end points. I. Thermodynamics and universality,” *Phys. Rev. B* **43**, 11177–11184 (1991).
- [9] David R. Nelson, J. M. Kosterlitz, and Michael E. Fisher, “Renormalization-Group Analysis of Bicritical and Tetracritical Points,” *Phys. Rev. Lett.* **33**, 813–817 (1974).
- [10] Martin Hasenbusch and Ettore Vicari, “Anisotropic perturbations in three-dimensional $O(N)$ -symmetric vector models,” *Phys. Rev. B* **84**, 125136 (2011).
- [11] Pasquale Calabrese, Andrea Pelissetto, and Ettore Vicari, “Multicritical phenomena in $O(n_1) \oplus O(n_2)$ -symmetric theories,” *Phys. Rev. B* **67**, 054505 (2003).
- [12] K. Sawada, “Variational Ground-State Energy of a Bose System. II,” *Phys. Rev.* **148**, 160–162 (1966).
- [13] Wilhelm Zwerger, “Quantum-unbinding near a zero temperature liquid-gas transition,” *J. Stat. Mech.* **2019**, 103104 (2019).
- [14] F. J. Gómez and J. Sesma, “Scattering length for Lennard-Jones potentials,” *Eur. Phys. J. D* **66**, 6 (2012).
- [15] R. A. Aziz, V. P. S. Nain, J. S. Carley, W. L. Taylor, and G. T. McConville, “An accurate intermolecular potential for helium,” *J. Chem. Phys.* **70**, 4330–4342 (1979).
- [16] Ronald A. Aziz, Frederick R.W. McCourt, and Clement C.K. Wong, “A new determination of the ground state interatomic potential for He_2 ,” *Mol. Phys.* **61**, 1487–1511 (1987).
- [17] Aurel Bulgac, “Dilute Quantum Droplets,” *Phys. Rev. Lett.* **89**, 050402 (2002).
- [18] D. S. Petrov, “Three-Body Interacting Bosons in Free Space,” *Phys. Rev. Lett.* **112**, 103201 (2014).
- [19] D. S. Petrov, “Quantum Mechanical Stabilization of a Collapsing Bose-Bose Mixture,” *Phys. Rev. Lett.* **115**, 155302 (2015).
- [20] L. Chomaz, S. Baier, D. Petter, M.J. Mark, F. Wächtler, L. Santos, and F. Ferlaino, “Quantum-Fluctuation-Driven Crossover from a Dilute Bose-Einstein Condensate to a Macro-

- droplet in a Dipolar Quantum Fluid,” *Phys. Rev. X* **6**, 041039 (2016).
- [21] Igor Ferrier-Barbut, Holger Kadau, Matthias Schmitt, Matthias Wenzel, and Tilman Pfau, “Observation of Quantum Droplets in a Strongly Dipolar Bose Gas,” *Phys. Rev. Lett.* **116**, 215301 (2016).
- [22] C. R. Cabrera, L. Tanzi, J. Sanz, B. Naylor, P. Thomas, P. Cheiney, and L. Tarruell, “Quantum liquid droplets in a mixture of Bose-Einstein condensates,” *Science* **359**, 301–304 (2017).
- [23] Shina Tan, “Three-boson problem at low energy and implications for dilute Bose-Einstein condensates,” *Phys. Rev. A* **78**, 013636 (2008).
- [24] Shangguo Zhu and Shina Tan, “Three-body scattering hypervolumes of particles with short-range interactions,” (2017), [arXiv:1710.04147](https://arxiv.org/abs/1710.04147).
- [25] P. M. A. Mestrom, V. E. Colussi, T. Secker, G. P. Groeneveld, and S. J. J. M. F. Kokkelmans, “van der Waals Universality near a Quantum Tricritical Point,” *Phys. Rev. Lett.* **124**, 143401 (2020).
- [26] This can be seen from the formula [34]
- $$r_0 a^2 = 2 \int_0^\infty dr [(r - a)^2 - u^2(r)],$$
- where $u(r)$ is the solution to the radial Schrödinger equation $-u''(r) + \hbar^{-2}mV(r)u(r) = 0$ which vanishes at $r = 0$ and tends to $r - a + o(r)$ as $r \rightarrow \infty$. This is also how we have obtained the numerical estimate (34) for $r_0 a^2$.
- [27] Toshiki Tajima, “Muonic Superdense Matter and Channeled Beams,” *Muon Cat. Fusion* **1**, 257 (1987).
- [28] John Wheeler, “Nanosecond Matter,” in *Energy in Physics, War and Peace: A Festschrift Celebrating Edward Tellers 80th Birthday*, edited by Hans Mark and Lowell Wood (Kluwer, Dordrecht, The Netherlands, 1988) Chap. 10, pp. 266–290.
- [29] Isaac F. Silvera and Victor V. Goldman, “The isotropic intermolecular potential for H₂ and D₂ in the solid and gas phases,” *J. Chem. Phys.* **69**, 4209–4213 (1978).
- [30] U. Buck, F. Huisken, A. Kohlhase, D. Otten, and J. Schaefer, “State resolved rotational excitation in D₂+H₂ collisions,” *J. Chem. Phys.* **78**, 4439–4450 (1983).
- [31] J. Pade, “Exact scattering length for a potential of Lennard-Jones type,” *Eur. Phys. J. D* **44**, 345–350 (2007).
- [32] S. A. Moskalenko and D. W. Snoke, *Bose-Einstein Condensation of Excitons and Biexcitons*, 2nd ed. (Cambridge, Oxford, UK, 2000).
- [33] Massimo Boninsegni, Youssef Kora, Dam Thanh Son, and Shiwei Zhang, to appear (2020).
- [34] Roger G. Newton, *Scattering Theory of Waves and Particles*, 2nd ed. (Springer, New York, NY, 1982).

Appendix A: Suppression of thermal non-tadpole diagrams

In our derivation of the three-dimensional effective field theory we have evaluated only the tadpole diagrams. We now show that non-tadpole graphs are suppressed.

Take as an example the correction to g_{eff} from the one-loop diagrams with two g' -vertices

$$\Delta g = -\frac{g'^2}{\beta} \sum_{n \neq 0} \int_{\mathbf{k}} \mathbf{k}^4 \left[\frac{1}{\left(\frac{2\pi n}{\beta}\right)^2 + \left(\frac{\hbar^2 \mathbf{k}^2}{2m} - \mu\right)^2} + \frac{4}{\left(\frac{-2\pi i n}{\beta} + \frac{\hbar^2 \mathbf{k}^2}{2m} - \mu\right)^2} \right]. \quad (\text{A1})$$

The n summation can be done, but it is easy to see that the result is parametrically

$$\Delta g = \frac{g'^2 \beta}{\lambda_T^7} F(-\beta\mu), \quad (\text{A2})$$

with some function F that is finite when $(-\beta\mu) \rightarrow 0$. In the regime under consideration

$$T \sim T_{\text{tri}} \sim \frac{\hbar^2}{m} \left(\frac{|a|}{\sigma^4}\right)^{2/3}, \quad \lambda_T \sim \left(\frac{\sigma^4}{|a|}\right)^{1/3}, \quad (\text{A3})$$

the correction is much smaller than the bare value

$$\Delta g \sim \frac{\hbar^2 |a|^{5/3}}{m \sigma^{2/3}} \sim \left(\frac{|a|}{\sigma}\right)^{2/3} g \ll g. \quad (\text{A4})$$

To proceed in a more general fashion, one can use the unit system with $\hbar = m = 1$, in which we can assign dimensions as in a nonrelativistic theory

$$[t] = -2, \quad [x] = [\lambda_T] = -1, \quad [\psi] = \frac{3}{2}, \quad [g] = -1, \quad [g'] = -3, \quad [G] = -4. \quad (\text{A5})$$

As integrating out modes with nonzero Matsubara frequency in the regime $\beta\mu \ll 1$ can bring out only powers of the thermal wavelength λ_T , the contribution to a quantity O of dimension Δ_O from a loop diagram containing N_g , $N_{g'}$, and N_G vertices of the respective types is of order

$$\frac{g^{N_g} g'^{N_{g'}} G^{N_G}}{\lambda_T^{\Delta_O + N_g + 3N_{g'} + 4N_G}} \sim \left(\frac{1}{\sigma}\right)^{\Delta_O} \left(\frac{|a|}{\sigma}\right)^{\frac{1}{3}\Delta_O + N_{g'} + \frac{4}{3}(N_g + N_G)} \quad (\text{A6})$$

Thus, the leading loop contribution to a given vertex is from the diagrams which minimize $N_{g'} + \frac{4}{3}(N_g + N_G)$. For example, the leading contribution to μ_{eff} comes from a diagram with $N_{g'} = 1$, $N_g = N_G = 0$, and the leading contribution to g_{eff} from a diagram with $N_G = 1$, $N_g = N_{g'} = 0$. These are tadpole diagrams. The non-tadpole diagrams are suppressed compared to the leading tadpole diagrams by at least $(a/\sigma)^{2/3}$. For example, from Eq. (A6) we find that the correction to g_{eff} coming from a diagram with two g' vertices ($N_{g'} = 2$) is suppressed compared by the tadpole diagram with $N_G = 1$ by a factor of $(|a|/\sigma)^{2/3}$, exactly as we have found in Eq. (A4).

Appendix B: Suppression of loops in the 3D effective field theory

So far we have treated the 3D effective field theory (52) classically. One can ask about the importance of loop corrections within this 3D theory. To answer that question we use

the unit system $\hbar = m_{\text{eff}} = 1$ and rewrite the 3D effective theory in Eq. (52) in the form (keeping also the higher-order term g')

$$\mathcal{L}_{3\text{D}}/\beta = \frac{1}{2}|\nabla\psi_0|^2 + \frac{1}{2}m_{3\text{D}}^2|\psi_0|^2 + \frac{g_{\text{eff}}}{2}|\psi_0|^4 + \frac{g'}{2}(\nabla|\psi_0|^2)^2 + \frac{G}{6}|\psi_0|^6, \quad (\text{B1})$$

where

$$m_{3\text{D}}^2 = \mu_{\text{eff}} \sim \frac{a^2}{\sigma^4}. \quad (\text{B2})$$

The dimensionless coupling constants controlling the loop corrections in the 3D theory are given by

$$\frac{g_{\text{eff}}T}{m_{3\text{D}}} \sim \left(\frac{|a|}{\sigma}\right)^{2/3}, \quad g'Tm_{3\text{D}} \sim \left(\frac{|a|}{\sigma}\right)^{5/3}, \quad GT^2 \sim \left(\frac{|a|}{\sigma}\right)^{4/3}, \quad (\text{B3})$$

and are all small in the regime $|a|/\sigma \ll 1$ we consider.

One can also ask if the higher-derivative or higher-order terms contribute to the surface tension calculated in Section III D. To answer that question we need to count powers of the field as $|\psi_0|^2 = n_{\text{cond}} \sim a/\sigma^4$ and each gradient as $\nabla \sim 1/\xi \sim a/\sigma^2$. Thus, for example, the contribution of the derivative interaction term in Eq. (B1) can be estimated as

$$g'(\nabla|\psi_0|^2)^2 \sim \frac{1}{\sigma^5} \left(\frac{|a|}{\sigma}\right)^4, \quad (\text{B4})$$

which is suppressed compared to the contribution of all other terms in Eq. (B1) such as, e.g., $G|\psi_0|^6 \sim (1/\sigma^5)(|a|/\sigma)^3$.